Interrogating the Configuration Space of Postbuckled Beams

Charles Cervi[1]; Sophia T. Santillan[2]; and Lawrence N. Virgin[3]

Abstract: This paper considers the global configuration space of postbuckled structures. Initially, a slender buckled beam is considered. The boundary conditions are pinned at one end and fully fixed at the other. The pin-end of the initially flat beam is moved toward the other end by a small amount. This causes the beam to buckle laterally (the beam is axially inextensional) with a characteristic shape. Since this is the outcome of a stable-symmetric pitchfork bifurcation, the buckled shape possesses a near mirror-image shape on the other side. Which of the two available equilibrium configurations is taken up depends on the usual, often small, symmetry-breaking effects commonly encountered in axially loaded systems. Given fixed conditions to maintain this initial buckled shape we then apply a moment at the pinned end. The relation between the applied moment and the change in shape is the primary focus of this study. The extent of the buckling (end shortening) is varied, with the magnitude of the moment, as a function of the angle, providing considerable information about the potential energy landscape in which the axially loaded system operates. The applied moment can be thought of as a probing mechanism whereby various equilibrium configurations are revealed, together with information regarding their stability and robustness. A similar approach is then used where the structure consists of two nominally identical beams attached at a right angle. In both cases, the opposite end from the actuation is clamped. An experimental study is conducted on 3D-printed specimens, and this is compared with a finite element analysis using ANSYS, and a large-deflection elastica analysis.
DOI: 10.1061/JENMDT.EMENG-6839.

Introduction

Reconfigurable structural systems exhibiting bistability have become popular recently. This is especially true in microelectrical mechanical systems (MEMS) applications including switches and actuators (Qiu et al. 2004; Nan et al. 2021), and metamaterials have shown the potential for structured configurations with highly desirable characteristics (Xia et al. 2019; Zhang et al. 2020; Deng et al. 2021). For the latter, 3D printing has facilitated the production of versatile and quite complicated elastic structural forms possessing distinct equilibrium configurations and exhibiting origami-like behavior and even materials with effective negative Poisson's ratio (Lakes 1993; Huang and Chen 2016). The ability to predict the buckling behavior of structural elements and hence influence or tailor their design is an important goal (Völlmecke et al. 2021).

We focus here on the moment actuation of a buckled beam. A similar system has been studied previously in the literature (Pan et al. 2022). The original contribution of this article is associated with moment actuation, reconstruction of the configuration space (using two carefully chosen points along the beam), and a comparison between FEA, elastica analysis (which we believe has not been applied to this type of problem before), and experimental data.

The analysis is extended to a right-angle frame, which is a minor extension of the beam model. It exhibits a strong symmetry, at least under the conditions here, and provides an additional opportunity to acquire data and apply the analysis. This type of configuration is especially useful in applications associated with energy harvesting, switching, and compliant mechanisms in general. The ability to radically tune the stiffness of a system has clear advantages for bistable gripper design, for example (Tissot-Daguette et al. 2022).

Flat Configuration

Prior to any end-shortening, we have a linear elastic system, see Fig. 1(a). That is, a simple beam that is most readily analyzed using the beam stiffness matrix (Hughes 1987). The stiffness coefficient relating an applied end moment to its corresponding rotation is given by $4EI/L$, based on the standard cubic shape function, and shown in Fig. 1(b) (Hughes 1987). Given the simplicity of the linear stiffness, it can be useful in a practical context to estimate Young's modulus, since $E = (L/4I)(M/\theta)$. That is, given the cross section dimensions (and hence I) and the length of the beam L, the slope of the moment-rotation relation can be used to find an estimate for E. Based on experimental data to be described later, the estimated value of Young's modulus (for 3D-printer ABS thermoplastic), was consistent with values suggested in previous studies (Virgin 2017), i.e., $E = 2.1$ GPa.

The simple linear expression does not address the issue of whether the pin-end moves in the axial direction. If the translational position of the pin-end is held in position, then a stretching (membrane action) is quickly induced under end rotation. If the end of the beam is moved (relative to the other end and by the application of a compressive end force for example), this also becomes a highly nonlinear problem and is the focus of the current study. Previous research in buckling has a long history (Timoshenko and Gere 1961; Thompson and Hunt 1984), including limit-point buckling in which the stiffness of a structure gradually reduces to zero due to axial loading effects. Snap-through behavior and the classic saddle-node bifurcation underpin much of the research of a specific form of buckling in which the instability is typically accompanied by a

[1]Graduate Student, Dept. of Mechanical Engineering and Materials Science, Duke Univ., Durham, NC 27708. Email: charles.cervi@duke.edu
[2]Associate Professor, Dept. of Mechanical Engineering and Materials Science, Duke Univ., Durham, NC 27708. Email: sophia.santillan@duke.edu
[3]Professor, Dept. of Mechanical Engineering and Materials Science, Duke Univ., Durham, NC 27708 (corresponding author). ORCID: https://orcid.org/0000-0001-5990-0722. Email: l.virgin@duke.edu

Note. This manuscript was submitted on July 1, 2022; approved on November 29, 2022; published online on January 12, 2023. Discussion period open until June 12, 2023; separate discussions must be submitted for individual papers. This paper is part of the ***Journal of Engineering Mechanics***, © ASCE, ISSN 0733-9399.

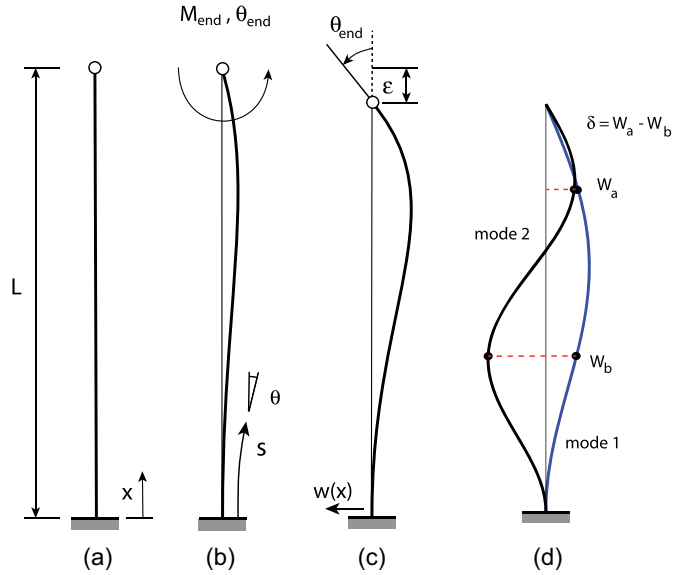

Fig. 1. (a) The clamped-pinned beam; (b) unbuckled deflected shape due to an end moment, M_{end}; (c) buckled, deflected shape due to end shortening, ϵ; and (d) the first two buckled modes.

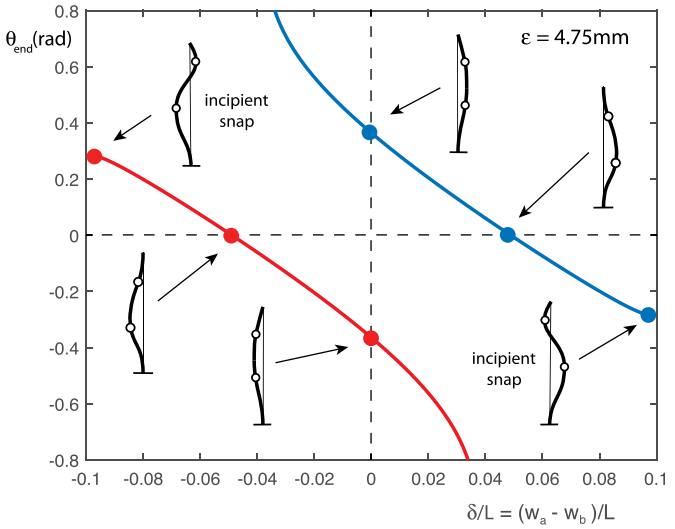

Fig. 2. Relation between the end angle θ, and the difference in lateral deflection δ for $\epsilon = 4.75$ mm $(\epsilon/L = 0.025)$ for a clamped-pinned beam. The small open circle symbols represent the measurement points.

sudden dynamic jump (as opposed to an often benign transition to a postbuckled state) (Virgin 2007; Taffetani et al. 2018; Zhong et al. 2018). There has been increased recent interest partly motivated by the probing of postbuckled equilibria (Thompson et al. 2017; Ehrhardt et al. 2020) and also the prospect of exploiting bistable structural behavior in micromechanical electrical systems (MEMS) (Camescasse et al. 2013; Tissot-Daguette et al. 2022; Wang et al. 2020; Pan et al. 2022) and metamaterials, with Cao et al. providing a recent review in this area (Cao et al. 2021).

Postbuckling

When one end of a thin, inextensional, prismatic flat beam is pushed toward the other end the end shortening ϵ is related to the lateral deflection W by the relation (Thompson and Hunt 1984):

$$\epsilon = L - \int_0^L (1 - W'^2)^{1/2} dX \tag{1}$$

where L = length of the beam [Fig. 1(c)]. For the boundary conditions at hand, the buckled mode shape is given by

$$W(X) = A\left[\frac{(L-X)}{L} - \frac{\sin(k(L-X))}{\sin(kL)}\right] \tag{2}$$

with $kL = 4.493$, obtained from solving $\tan kL - kL = 0$ (Chen and Lui 1987). Placing Eq. (2) into Eq. (1) and evaluating $W'(L)$ provides a purely quadratic relation between end-shortening and end angle. For example, an end-shortening of $\epsilon/L = 0.02$ results in an end angle of $\theta(L) \approx \pm 0.35$ rad, and the lateral deflection grows rapidly with end shortening. An elastica analysis, to be described later, gave very similar results. However, once the beam is buckled into a specific (nontrivial) deflected configuration with a new enforced equilibrium, symmetry is broken. We then apply a moment at the pinned end, and the problem becomes highly nonlinear, with snap-through inevitable (Plaut and Virgin 2009).

Projection of the Deflected Shape

The initial shape is described by the first buckling mode [Eq. (2)]. However, as an end moment is applied the beam deflects with the growth of a shape that contains a second-mode effect, especially just prior to the loss of stability at snap-through. This more complicated shape resembles Eq. (2) with $kL = 7.725$ (Chen and Lui 1987). The difficulty in experimentally measuring the end angle (to be described later), together with limited information about the spanwise shape, motivated the development of a pseudo measurement to represent the changing shape with a kind of higher modal influence. This was achieved by focusing on two points, $X = X_a$ and $X = X_b$, along the beam, that have lateral displacements $W(X_a) = W_a$ and $W(X_b) = W_b$, respectively. The values X_a and X_b were determined such that they best represent the first two mode shapes, i.e., for the first buckling mode, $W_a - W_b \approx 0$, with $W_a - W_b$ as large as possible when the beam is primarily in the second-mode shape, see Fig. 1(d). Although by no means exact, the locations $X_a = 0.79L$ and $X_b = 0.38L$ give an effective measure, or projection, of the deflected shape [Fig. 1(d)] based on this limited sampling. Thus, defining the quantity $\delta = W_a - W_b$ gives us significant additional information about the beam's shape. This is tantamount to a conventional finite difference approximation based on discrete data.

Using these representative points, plotting δ vs other variables, we can observe the progression toward snap-through, initially dominated by the first mode in the stable equilibrium ($\delta \approx 0$), and transitioning to a second-mode dominated shape as the structure is nearing snap-through, with δ near a maximum. Postsnap, the beam settles in a shape similar to the initial shape but on the other side. Fig. 2 shows the relation between the end angle, θ_{end}, and this second-mode measure, δ. The near-linear relation supports the use of this proxy (only stable paths are plotted in this figure), which is easily measured experimentally using two proximity lasers.

Initial Buckling

For a single column with clamped-pinned boundary conditions, the critical elastic buckling load is given by $P_{cr} \approx 20.1EI/L^2$ (Timoshenko and Gere 1961). That is, the Euler load adjusted for

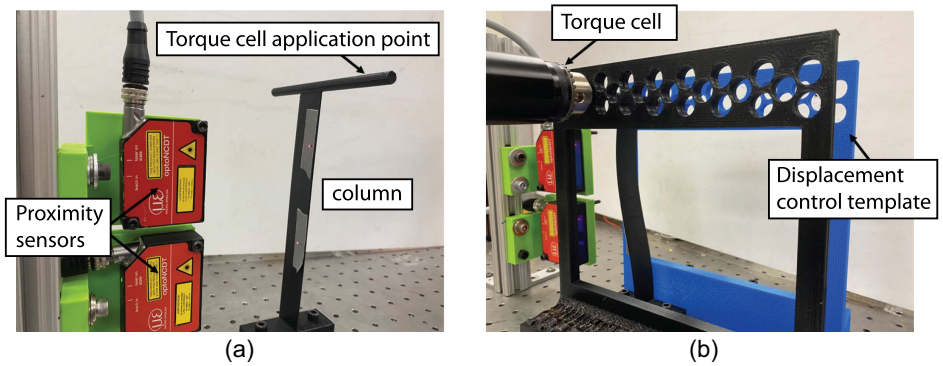

Fig. 3. Photographic image of the experimental column: (a) the two lasers used to measure lateral deflection at W_a and W_b; and (b) the template for the upper-end position.

an effective length of $0.7L$ for these end conditions, assuming a slender geometry, i.e., L/r is large, where $r = \sqrt{I/A}$, with $A = bd$, $I = bd^3/12$. For the dimensions of the experimental systems to be described later, we generally have $b = 25.4$ mm, $d = 1.36$ mm, $L = 188$ mm, giving a slenderness ratio of $L/r \approx 478$, i.e., *very* slender (Virgin 2007). Assuming a Young's modulus of $E = 2.1$ GPa, we expect a critical load in the vicinity of 6.3 N, and preliminary experimental tests indicated buckling close to this value.

Experimental Setup

Prior to data acquisition, the structure (which incorporated an integrally printed base) is fixed to an isolation table, as shown in Fig. 3. The other end of the structure is then placed inside two bearings that are locked into stands on each side of the structure to create a pinned boundary condition. The stands allow a consistent end-shortening to be applied, within the bearings and in prescribed vertical increments of 1 mm. A torque cell is then connected to the pinned end. To measure displacements, two microepsilon proximity sensors (OptoNCDT, Micro-Epsilon, Raleigh, North Carolina) are directed at the sampling points. Both the torque cell and laser displacement sensors are connected to a computer for simultaneous data acquisition via LabVIEW. During this process, the torque cell is first slowly rotated in the direction away from snap-through to collect data on the nonlinear stiffening of the structure. Then, the direction of the torque cell rotation is reversed and slowly rotated toward snap-through. Data collection is then stopped postsnap. Then, data collection is started again, and the process is repeated for the other side until it snaps back to the original position. This behavior is unambiguously hysteretic. The data are then compared to FEA and the Elastica model.

Analytical Formulation

Numerical Analysis—ANSYS

Finite element models were developed using ANSYS for both the beam and structure to characterize the nonlinear stiffening and snap-through behavior of the bistable structures. Tetrahedron elements were used with a mesh size set to 2.0 mm due to convergence and computational speed. A Young's modulus $E = 2.1$ GPa and $\nu = 0.39$ was utilized. The large-deflection capability of the software was activated for the entire simulation.

Four steps are employed in each analysis. The first three steps buckle the structure into the first stable buckling mode, and the fourth step applies the angle to trigger snap-through. In the first step, a lateral force is applied to the span of the beam. In the second step, the desired end shortening is applied to the pinned boundary condition. In the third step, the lateral force is removed to leave the stable buckled shape.

During the fourth step, an angle is imposed on the pinned boundary condition and swept through a range of values. The enforced angle is initially rotated away from snap-through to examine the nonlinear stiffening of the structure. Changing directions, the angle is then rotated to trigger the snap-through behavior. Reaction moments, as well as the displacements of two sampling points, are obtained from the simulations and compared to other models.

Elastica Analysis

The thin, uniform beam is depicted in Fig. 1 in both its undeflected and buckled configurations. It is considered inextensional, with length L, and constant bending stiffness EI. Points on the beam have coordinates $X(S,T)$ and $Y = W(S,T)$ and rotation $\theta(S,T)$ with respect to the X axis, where S is the arclength and T is time. The axial end-shortening of the beam is ϵ.

The internal forces in the beam are denoted, $P(S,T)$ and $Q(S,T)$ parallel to the X and Y axes, respectively, and the bending moment is $M(S,T)$. The governing equations, based on geometry, moment-curvature relation, and equilibrium are:

$$\partial X/\partial S = \cos\theta, \qquad \partial W/\partial S = \sin\theta,$$
$$\partial\theta/\partial S = M/EI, \qquad \partial M/\partial S = Q\cos\theta - P\sin\theta,$$
$$\partial P/\partial S = -(m_g)\partial^2 X/\partial T^2 \qquad \partial Q/\partial S = -(m_g)\partial^2 W/\partial T^2 \tag{3}$$

where m_g = mass per unit length.

The following nondimensional quantities are defined

$$x = X/L, \qquad w = W/L, \qquad s = S/L, \qquad t = (T/L^2)\sqrt{EI/m_g},$$
$$p = PL^2/EI, \qquad q = QL^2/EI, \qquad m = ML/EI \tag{4}$$

In nondimensional terms, Eq. (3) become

$$\partial x/\partial s = \cos\theta, \qquad \partial w/\partial s = \sin\theta,$$
$$\partial\theta/\partial s = m, \qquad \partial m/\partial s = q\cos\theta - p\sin\theta,$$
$$\partial p/\partial s = -\partial^2 x/\partial t^2, \qquad \partial q/\partial s = -\partial^2 w/\partial t^2 \tag{5}$$

At equilibrium, the equations are given by

$$x'_e = \cos\theta_e, \qquad w'_e = \sin\theta_e,$$
$$\theta'_e = m_e, \qquad m'_e = q_e\cos\theta_e - p_e\sin\theta_e \tag{6}$$

where primes denote derivatives with respect to arclength, and the internal forces are

$$p_e(s) = p_o, \qquad q_e(s) = q_o \tag{7}$$

with p_0 and q_0 representing values at $s = 0$ (Santillan et al. 2005; Chen and Tsao 2013).

For a given nondimensional end-shortening, ϵ/L, we then choose either $\theta_{\text{end}} = \theta_e(1)$ or $m_{\text{end}} = m_e(1)$ as the control parameter to follow a solution path and use a shooting method with the known boundary conditions, $x_e(0) = w_e(0) = \theta_e(0) = w_e(1) = 0$, $x_e(1) = 1 - \epsilon/L$, and $\theta_e(1) = \theta_{\text{end}}$ or $m_e(1) = m_{\text{end}}$, to find equilibrium solutions.

The stability of the equilibrium configurations is determined by computing the frequencies of small amplitude vibrations (Santillan et al. 2005). To do so, the nondimensional variables (which are now functions of arclength and time) are written

$$x(s,t) = x_e(s) + x_d(s)\sin\Omega t, \qquad w(s,t) = w_e(s) + w_d(s)\sin\Omega t,$$
$$\theta(s,t) = \theta_e(s) + \theta_d(s)\sin\Omega t, \qquad m(s,t) = m_e(s) + m_d(s)\sin\Omega t,$$
$$p(s,t) = p_o + p_d(s)\sin\Omega t, \qquad q(s,t) = q_o + q_d(s)\sin\Omega t \tag{8}$$

where the nondimensional frequency, Ω, is defined

$$\Omega = \omega L^2\sqrt{m_g/EI} \tag{9}$$

and ω = dimensional frequency. These expressions, using Eqs. (5), (6), and (8), result in the following dynamic variable equations

$$x'_d = \theta_d\sin\theta_e, \qquad w'_d = \theta_d\cos\theta_e,$$
$$\theta'_d = m_d, \qquad m'_d = (q_d - p_o\theta_d)\cos\theta_e - (p_d + q_o\theta_d)\sin\theta_e,$$
$$p'_d = \Omega^2 x_d, \qquad q'_d = \Omega^2 w_d \tag{10}$$

Again, for a given equilibrium configuration, a shooting method is used with the known boundary conditions, $x_d(0) = w_d(0) = \theta_d(0) = x_d(1) = w_d(1) = \theta_d(1) = 0$ and an arbitrary, small value for $m_d(0)$ to find the first vibration mode and corresponding vibration frequency, Ω_1.

Right-Angled Frame

We next consider a right-angled frame that in many ways is very similar to the column, but consists of two columns inclined at 45 degrees and joined at their apex, the point at which a vertical load, or end-shortening, is applied. An image of the experimental setup is shown in Fig. 4.

We can again consider the initial buckling behavior of this structural arrangement. A useful approximate approach, well-suited to the current application, was developed by Newmark (Newmark 1949), to take account of the effect of elastic end-restraint. It was shown that a close approximation to the buckling load of a column with elastic end restraints is given by

$$P_{cr} = \frac{\pi^2 EI}{L^2}\left[\frac{(0.4+\lambda_a)(0.4+\lambda_b)}{(0.2+\lambda_a)(0.2+\lambda_b)}\right] \tag{11}$$

where $\lambda_a = EI/(C_1 L)$ and $\lambda_b = EI/(C_2 L)$, and where C_1 and C_2 represent rotational spring constants at the ends. This enables bracketing of anticipated buckling behavior in a situation where a boundary condition is somewhat intermediate between pinned and clamped in an experimental support. For example, with clamped ends corresponding to $C_1 = C_2 = \infty$ and thus $\lambda_a = \lambda_b = 0$, we obtain $P_{cr} = 4\pi^2 EI/L^2$, with and pinned ends corresponding to $C_1 = C_2 = 0$ and thus $\lambda_a = \lambda_b = \infty$, we obtain $P_{cr} = \pi^2 EI/L^2$, for an isolated (Euler) column.

A schematic of the frame is shown in Fig. 5. The initial buckled configuration is not symmetric with respect to the postbuckled equilibria. This occurs because as the buckled shape grows, there is an uneven distribution of resistance to the loading, and this will be further discussed in the "Results" section.

For the right-angled frame, the lower ends of the two columns are clamped and the upper ends have some elastic constraint, and the axial load is shared between the two columns. In similarity with the single clamped-hinged column, we would expect a frame buckling load somewhat between these two extremes. The rotational stiffness provided by the adjacent beam at the upper end is $C_2 = 4EI/L$ (a right angle is maintained at the apex). Using Eq. (11), we would thus expect a buckling load close to $P_{cr} \approx 29EI/L^2$, a value confirmed using ANSYS, and consistent with an estimate based on experimental data.

A similar elastica analysis is carried out here as well, where each equilibrium variable is integrated along the two nondimensional arclengths, s_1 and s_2, and again, a shooting method is used with a prescribed upper joint rotation angle, θ_{end}. Here, the known boundary conditions are

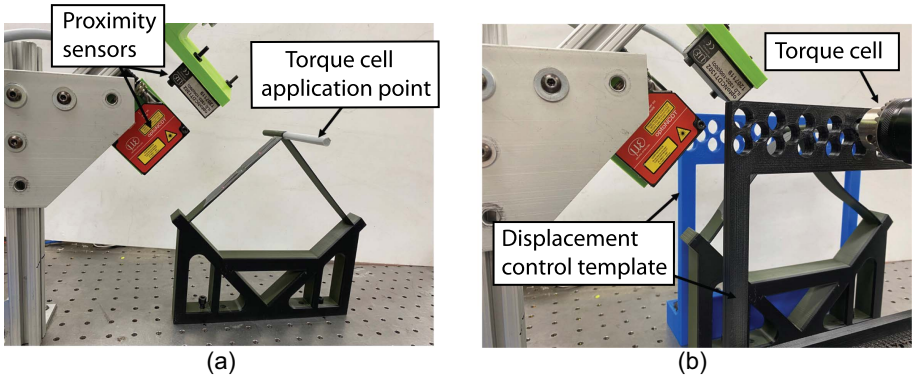

Fig. 4. Photographic image of the experimental frame: (a) the two lasers used to measure lateral deflection at W_a and W_b; and (b) the template for the upper-end position.

J. Eng. Mech., 2023, 149(3): 04023009

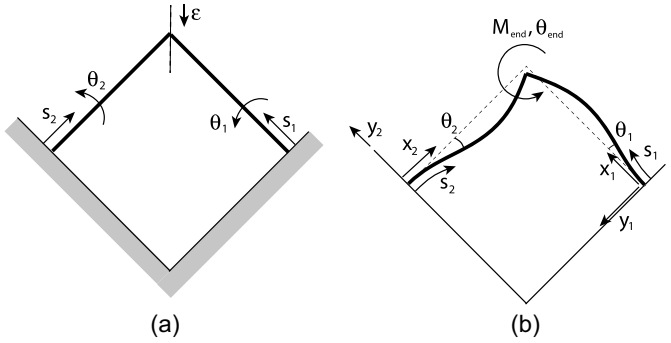

Fig. 5. A schematic of the right-angled frame: (a) the coordinate system; and (b) buckled configuration (after the connected joint is subject to a symmetric 'end' displacement ϵ).

$$x_{1e}(0) = w_{1e}(0) = \theta_{1e}(0) = 0, \qquad x_{2e}(0) = w_{2e}(0) = \theta_{2e}(0) = 0,$$
$$w_{1e}(1) = \frac{\epsilon}{\sqrt{2}L}, \qquad w_{2e}(1) = -\frac{\epsilon}{\sqrt{2}L},$$
$$x_{1e}(1) = x_{2e}(1) = 1 - \frac{\epsilon}{\sqrt{2}L}, \qquad \theta_{1e}(1) = \theta_{2e}(1) = \theta_{\text{end}} \tag{12}$$

A stability analysis is also conducted here, resulting in the same dynamic variable equations as in the column analysis. Here, the known boundary conditions are

$$x_{1d}(0) = w_{1d}(0) = \theta_{1d}(0) = 0, \qquad x_{2d}(0) = w_{2d}(0) = \theta_{2d}(0) = 0,$$
$$x_{1d}(1) = w_{1d}(1) = \theta_{1d}(1) = 0, \qquad x_{2d}(1) = w_{2d}(1) = \theta_{2d}(1) = 0 \tag{13}$$

Results

Column

The estimated buckling load for the column is $P_{cr} \approx 20EI/L^2 = 6.3$ N based on an ideal geometry and assumed material properties, and although buckling loads were not measured directly, this value is not inconsistent with an approximate measurement. The elastica approach gave a buckling load of $20.19EI/L^2$.

For the case of $\epsilon = 4.75$ mm ($\epsilon/L = 0.025$), Fig. 6 shows the relation between the various deflection parameters as the pinned end is subject to a moment. Starting from an initial buckled shape corresponding approximately to $W_a = W_b = \pm 14$ mm, $\delta \approx 0$, the end rotation proceeds until a snap event occurs, when the system suddenly jumps to the remote mirror-image solution. These are indicated by the arrows. There is excellent agreement between FEA, elastica analysis, and the experimental data.

Fig. 7 shows the moment - δ relation for this same case. The resolution of the torque cell was limited to 0.005 N-m, and this can be observed in the granularity of the vertical axis data. Although the qualitative agreement between the experimental data and analyses is very good, the experimental moments are somewhat less than

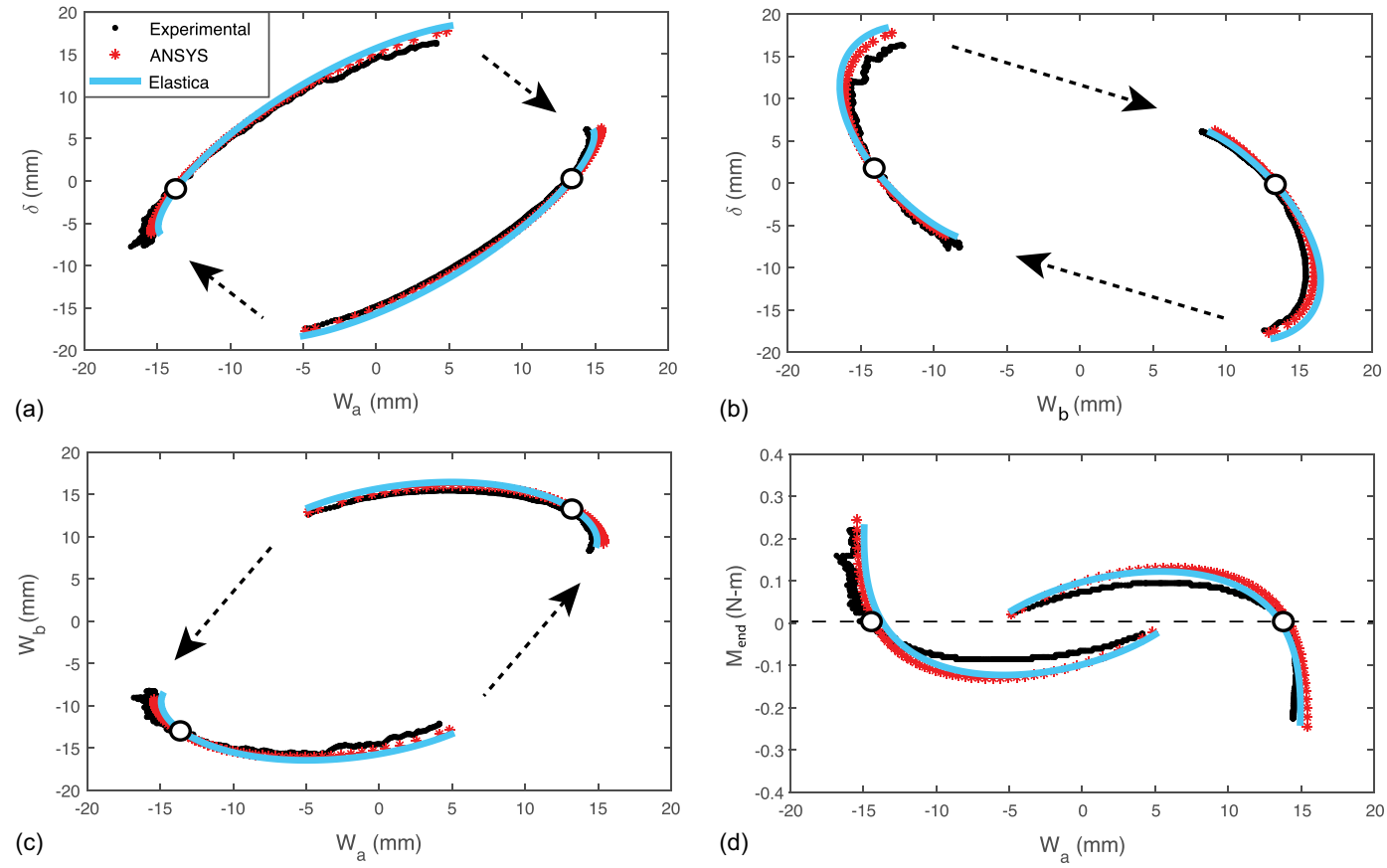

Fig. 6. A comparison between analysis, FEA (ANSYS), and experimental data for a clamped-pinned beam, for $\epsilon = 4.75$ mm ($\epsilon/L = 0.025$): (a) δ versus W_a; (b) δ versus W_b; (c) W_b versus W_a; and (d) M_{end} versus W_a.

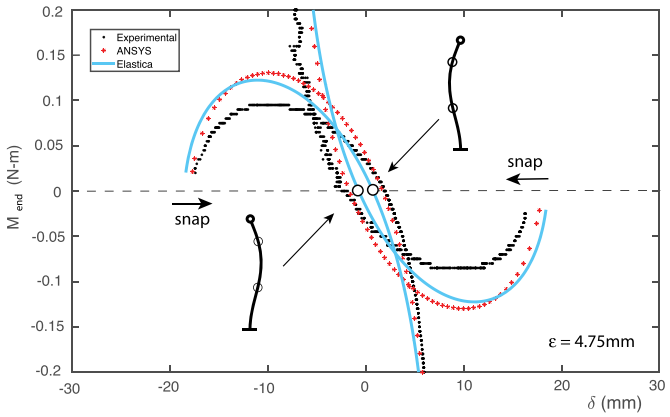

Fig. 7. A comparison between analysis, FEA (ANSYS), and experimental data for $\epsilon = 4.75$ mm ($\epsilon/L = 0.025$). M_{end} versus δ.

expected. This could be a result of typical experimental issues related to modeling, manufacturing, material properties, and tolerances.

If the end of the column has moved a distance of 6.75 mm ($\epsilon/L = 0.036$) toward the other end of the column, we have a more heavily buckled system. Applying an end moment to this initial configuration leads to the results shown in Fig. 8. Again, there is excellent agreement between theory and experiment. The $M - \delta$ relation for this case is shown in Fig. 9. It should be noted that in both the elastica analysis and FEA the solution becomes unstable at the snap instability. This is a classic saddle-node, or fold, instability (Virgin 1986). At the other end of each equilibrium path, as the angle is moved away from a snap, the corresponding applied moment becomes very large (stretching) and the experiment and both sets of analyses are simply terminated.

In contrast to the experiment and ANSYS, the elastica approach provides complete equilibrium paths including unstable branches, but, again, here only stable paths are shown. The stability of the equilibrium configurations is determined using vibration analysis in the elastica approach, as detailed earlier. Fig. 10 shows how the lowest (nondimensional) natural frequency Ω varies with the end angle (θ_{end}) and nondimensional end moment (m_{end}), and the corresponding change in shape: the sequence labeled $1 \rightarrow 6$, with the snap instability occurring as the frequency (and hence stiffness) drops to zero. We draw attention to some specific shapes. The point ($m_{\text{end}} = 0$, $\theta_{\text{end}} = 0.48$) corresponds to the initial buckled shape, i.e., when the ends are moved together by $\epsilon/L = 0.036$, causing the pinned end to rotate prior to the application of an external end moment. Also, the open circle data points indicate the case of zero end angle, and the end moment required to maintain it in that specific position ($\theta_{\text{end}} = -0.24$). A subtle feature of stability analysis depends on which parameter is prescribed and which is solved for. This is related to the alternatives of applying a moment-controlled actuation or angle-controlled actuation and subsequent instability (often at a tangency in the response) (Tissot-Daguette et al. 2022). It is interesting to observe that the snap buckling occurs just prior to the applied moment dropping to zero.

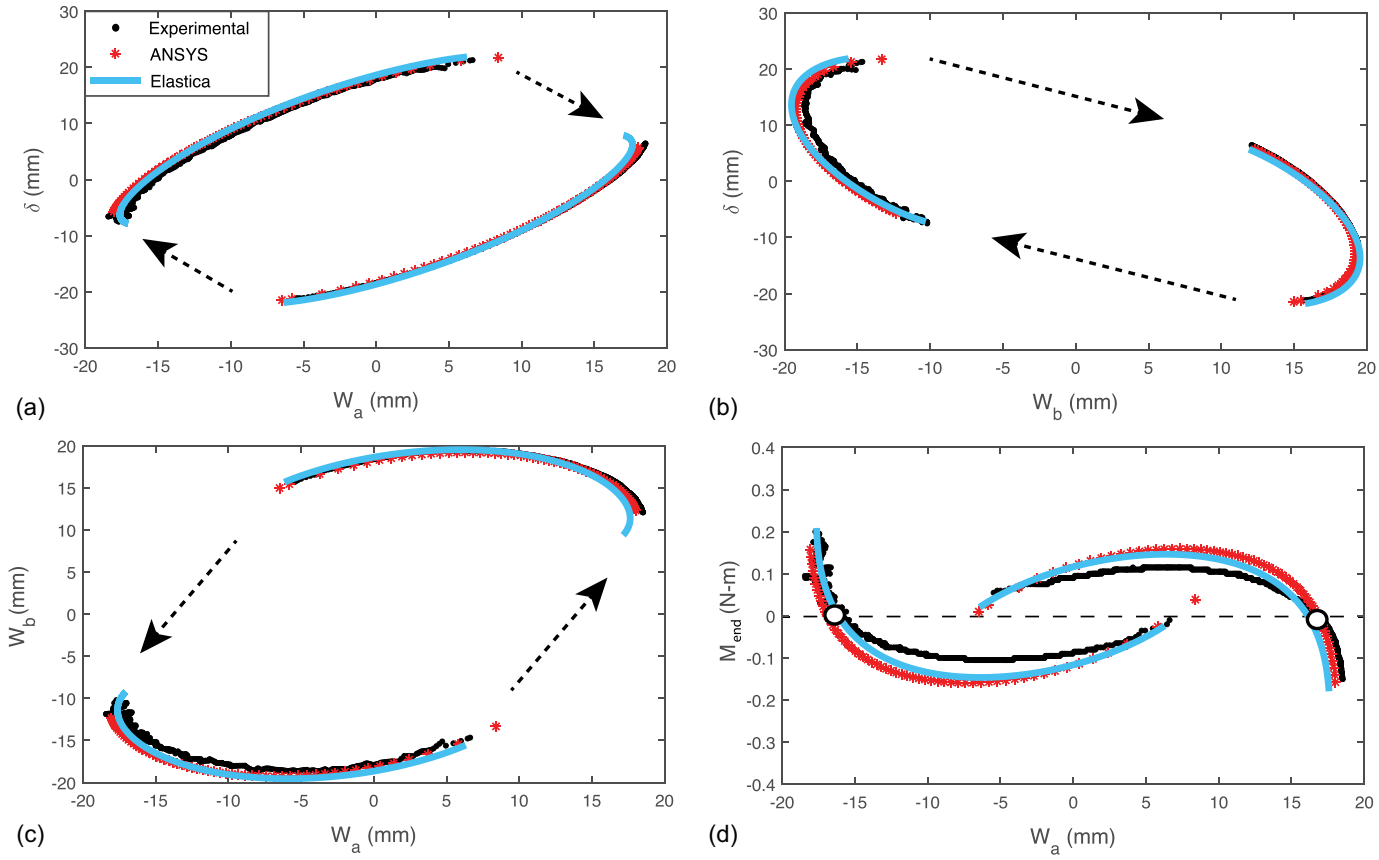

Fig. 8. A comparison between analysis, FEA (ANSYS), and experimental data for a clamped-pinned beam for $\epsilon = 6.75$ mm ($\epsilon/L = 0.036$): (a) δ versus W_a; (b) δ versus W_b; (c) W_b versus W_a; and (d) M_{end} versus W_a.

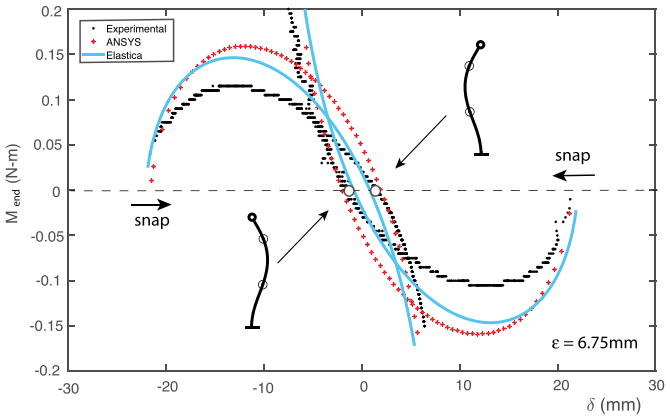

Fig. 9. A comparison between analysis, FEA (ANSYS), and experimental data for $\epsilon = 6.75$ mm ($\epsilon/L = 0.036$). M_{end} versus δ.

Following these sometimes convoluted solutions numerically requires special techniques, especially if unstable solutions ($\Omega^2 < 0$) are followed (Yang et al. 2007). We should also mention that there has been some recent progress in using continuation to follow unstable paths experimentally (Sieber et al. 2008; Barton and Burrow 2010; Neville et al. 2018).

Right-Angled Frame

In similarity with the isolated postbuckled column, the estimated buckling load for the postbuckled right-angled frame is $P_{cr} \approx 29EI/L^2 = 7.3$ N, based on Eq. (11) (and ANSYS). Note, the member lengths and thicknesses are different from the single column and thus the buckling loads are not directly comparable. The elastica analysis gave a buckling load of $28.55EI/L^2$.

Similar results are shown for the right-angled frame in Fig. 11, in which the corner of the frame is moved symmetrically downward (i.e., diagonally) by an amount of 6.25 mm. In this case, the length of each column is 140 mm, and the thickness of each column is 1.04 mm. The relation between M and δ is shown in Fig. 12. Again, characterizing the shapes using the lateral deflection at two points, as indicated in the figure, provides a useful description of the change in shape under the moment applied at the corner. Not only is the moment-shape relation very similar in the experiment and analysis, the points of snap from both results are comparable. Similar to the column, we see a consistent overestimation of the end moment during snap through, likely a result of the issues discussed about the column.

It is interesting to observe the asymmetry in the deflection. The frame is quite highly buckled (see the insets in Fig. 12), so, for example, the two values of W_a at the free equilibrium (when $M = 0$), corresponding to each direction of initial buckling, are approximately -15 mm and 7 mm. This is caused by the manner in which the load direction is oriented relative to the two buckled shapes. It is also apparent in Fig. 11 in which the two equilibria are not symmetric about $\delta = 0$, and the snap occurs from somewhat different shapes, as signified again by different magnitudes of δ values. By comparison, the buckled column exhibits symmetry as seen in Figs. 6–9, where results are symmetric about $W_a = 0$ and $\delta = 0$.

Conclusions

Interrogating the postbuckled equilibrium configurations of structures provides useful information, especially if the structure is subsequently subject to intense dynamic excitation, for example. The current study focuses on the relationship between a moment applied at one end of a column (already buckled) and its corresponding deflected shape. Given the postbuckled and highly nonlinear nature of the response, we observe an interesting transition from a mode-one-dominated shape to a mode-two-dominated shape prior to a sudden snap between equilibrium shapes. This is classic bistable behavior. Similar results were also obtained for a right-angled frame compressed along its axis of symmetry. The experimental data exhibited close agreement with FEA using the ANSYS package, as well as an elastica analysis using large-deflection arclength coordinates. The correlation between theory and experiment is excellent, not only for the equilibrium shapes but also in terms of the loss of stability.

This modeling was successful and provides a strong resource for the design of bistable structural systems that can be used in switches, energy harvesting, and grippers.

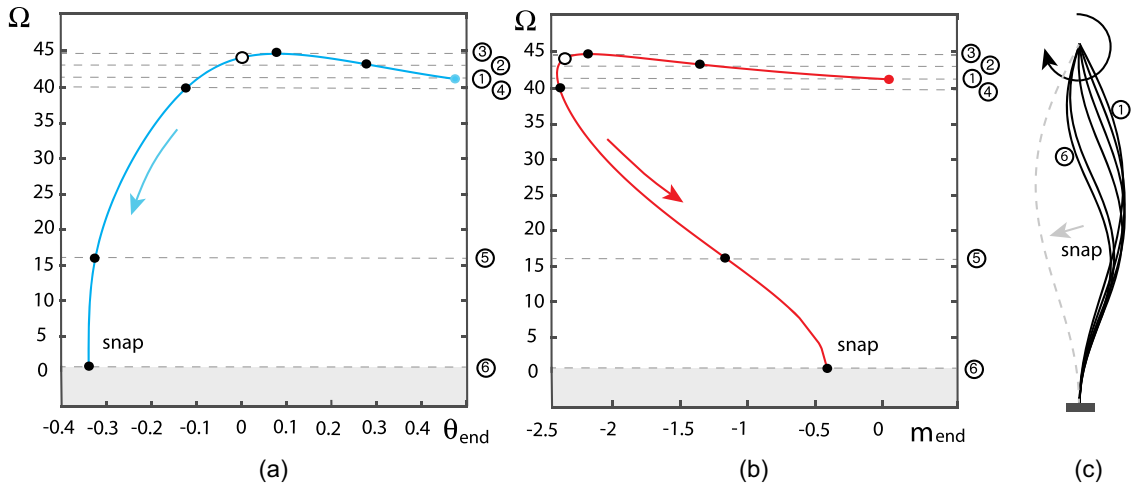

Fig. 10. The stability of the equilibrium shapes (lowest vibration frequency) as a function of (a) end angle; (b) end moment (under changing end angle); and (c) snapshots of representative shapes $\epsilon = 6{:}75$ mm ($\epsilon/L = 0.036$).

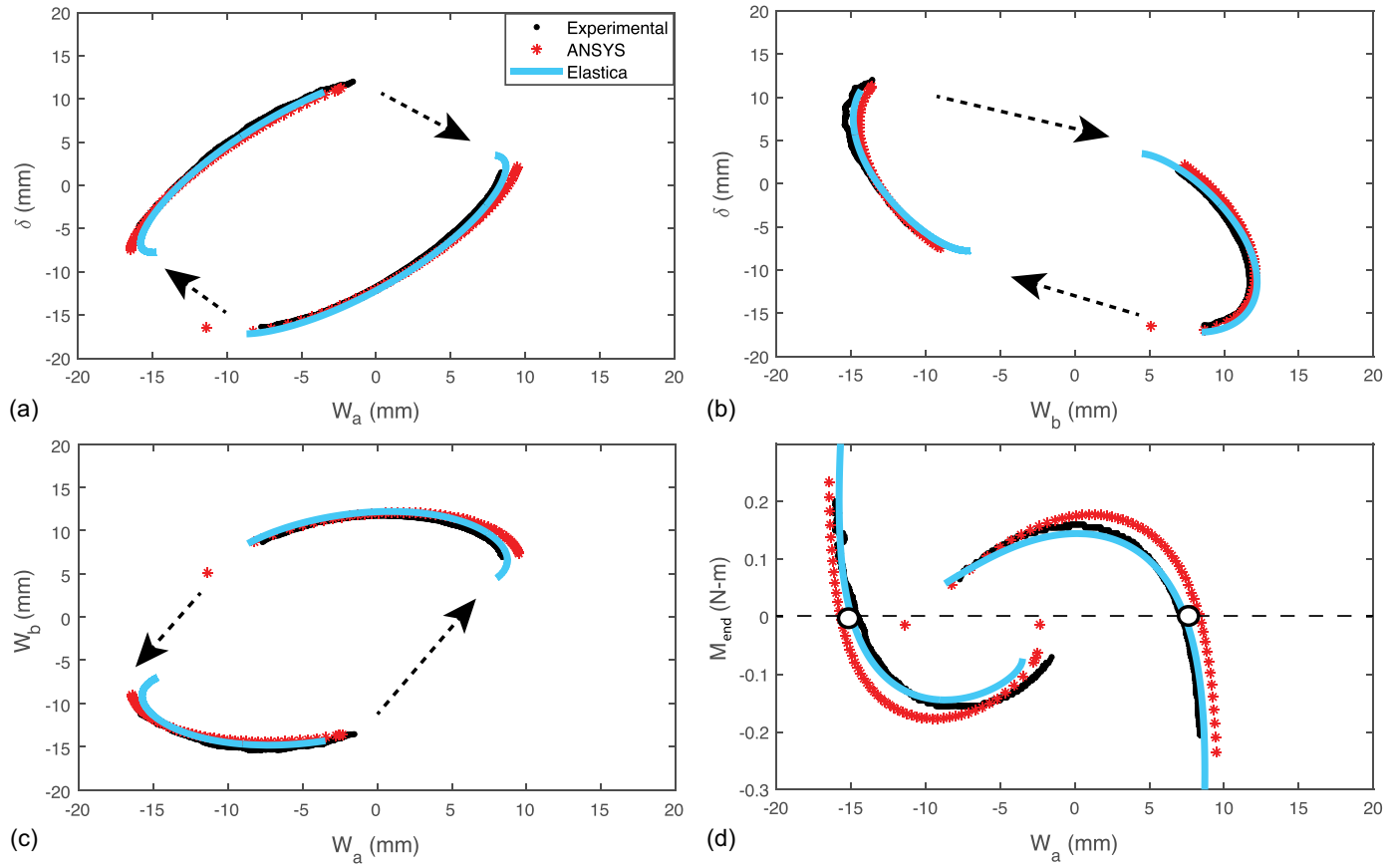

Fig. 11. A comparison between analysis, FEA (ANSYS), and experimental data for the right-angled frame for $\epsilon = 6.25$ mm: (a) δ versus W_a; (b) δ versus W_b; (c) W_b versus W_a; and (d) M_{end} versus W_a.

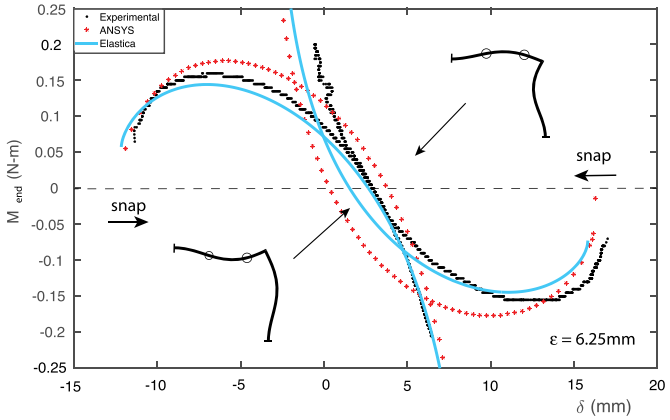

Fig. 12. A comparison between analysis, FEA (ANSYS), and experimental data for the right-angled frame for $\epsilon = 6.25$ mm. M_{end} versus δ.

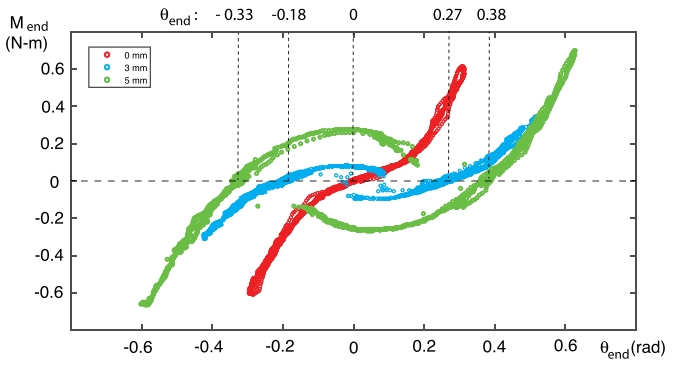

Fig. 13. Preliminary moment-angle experimental data for three cases: $\epsilon = 0$; 3; 5 mm, progressively into the postbuckled regime.

Appendix. Moment-angle Relation

As mentioned in the text, the deflected shape was inferred using the measurement of lateral translation at two locations, rather than a direct measurement of the end angle. A preliminary study, albeit with lower accuracy and measurement resolution, is briefly presented here for completeness.

Fig. 13 shows the moment-angle relation based on experimental data for three end-shortenings for a slightly different geometric column. The data are the result of a number of sweeps (traverses through end angle) and the data superimposed. It is interesting to see the unbuckled case (0 mm end-shortening) with the initial linear response soon giving way to a stiffening response due to stretching. Some of the geometric parameters for this early study were not the same used as in the main study described in this paper. It is also interesting to note the asymmetry in the 3 mm end-shortening case.

This mildly buckled case exhibits a very low stiffness and a degree of uncertainty in the locations of the equilibrium configurations.

Data Availability Statement

All data, models, or code that support the findings of this study are available from the corresponding author upon reasonable request.

Acknowledgments

This research was supported with funding from the NSF (CMMI 1926672). The opinions, findings, and conclusions or recommendations expressed are those of the author(s) and do not necessarily reflect the views of the National Science Foundation.

References

Barton, D. A. W., and S. G. Burrow. 2010. "Numerical continuation in a physical experiment: Investigation of a nonlinear energy harvester." *J. Comput. Nonlinear Dyn.* 6 (1): 011010. https://doi.org/10.1115/1.4002380.

Camescasse, B., A. Fernandes, and J. Pouget. 2013. "Bistable buckled beam: Elastica modeling and analysis of static actuation." *Int. J. Solids Struct.* 50 (19): 2881–2893. https://doi.org/10.1016/j.ijsolstr.2013.05.005.

Cao, Y., M. Derakhshani, Y. Fang, G. Huang, and C. Cao. 2021. "Bistable structures for advanced functional systems." *Adv. Funct. Mater.* 31 (45): 2106231. https://doi.org/10.1002/adfm.202106231.

Chen, J.-S., and H.-W. Tsao. 2013. "Static snapping load of a hinged extensible elastic." *Appl. Math. Modell.* 37 (18): 8401–8408. https://doi.org/10.1016/j.apm.2013.03.040.

Chen, W. F., and E. M. Lui. 1987. *Structural stability: Theory and implementation*. Amsterdam, Netherlands: Elsevier.

Deng, B., J. R. Raney, K. Bertoldi, and V. Tournat. 2021. "Nonlinear waves in flexible mechanical metamaterials." *J. Appl. Phys.* 130 (4): 040901. https://doi.org/10.1063/5.0050271.

Ehrhardt, D., L. N. Virgin, and S. M. Spottswood. 2020. "Experiments on probing the configuration space of post-buckled panels." *J. Appl. Mech.* 87 (12): 121005. https://doi.org/10.1115/1.4048197.

Huang, C., and L. Chen. 2016. "Negative Poisson's ratio in modern functional materials." *Adv. Mater.* 28 (37): 8079–8096. https://doi.org/10.1002/adma.201601363.

Hughes, T. 1987. *The finite element method*. Englewood Cliffs, NJ: Prentice-Hall.

Lakes, R. 1993. "Advances in negative Poisson's ratio materials." *Adv. Mater.* 5 (4): 293–296. https://doi.org/10.1002/adma.19930050416.

Nan, W., H. Yuncheng, and F. Jiyang. 2021. "Bistable energy harvester using easy snap-through performance to increase output power." *Energy* 226 (Jul): 120414. https://doi.org/10.1016/j.energy.2021.120414.

Neville, R. M., R. M. J. Groh, A. Pirrera, and M. Schenk. 2018. "Shape control for experimental continuation." *Phys. Rev. Lett.* 120 (25): 254101. https://doi.org/10.1103/PhysRevLett.120.254101.

Newmark, N. M. 1949. "A simple approximation formula for effective end-fixity of columns." *J. Aeronaut. Sci.* 16 (2): 116. https://doi.org/10.2514/8.11738.

Pan, D., Y. Shen, C. Huang, and Z. Wu. 2022. "Analysis of snap-through behavior of bistable buckled beam under end-moment static actuation." *Int. J. Non Linear Mech.* 142 (Jun): 103937. https://doi.org/10.1016/j.ijnonlinmec.2022.103937.

Plaut, R. H., and L. N. Virgin. 2009. "Vibration and snap-through of bent elastica strips subjected to end rotations." *J. Appl. Mech.* 76 (4): 041011. https://doi.org/10.1115/1.3086783.

Qiu, J., J. H. Lang, and A. H. Slocum. 2004. "A curved-beam bistable mechanism." *J. Microelectromech. Syst.* 13 (2): 137–146. https://doi.org/10.1109/JMEMS.2004.825308.

Santillan, S. T., L. N. Virgin, and R. H. Plaut. 2005. "Post-buckling and vibration of heavy beam on horizontal or inclined rigid foundation." *J. Appl. Mech.* 73 (4): 664–671. https://doi.org/10.1115/1.2165237.

Sieber, J., A. Gonzalez-Buelga, S. A. Neild, D. J. Wagg, and B. Krauskopf. 2008. "Experimental continuation of periodic orbits through a fold." *Phys. Rev. Lett.* 100 (24): 244101. https://doi.org/10.1103/PhysRevLett.100.244101.

Taffetani, M., X. Jiang, D. P. Holmes, and D. Vella. 2018. "Static bistability of spherical caps." *Proc. R. Soc. A* 474 (2213): 20170910. https://doi.org/10.1098/rspa.2017.0910.

Thompson, J. M. T., and G. W. Hunt. 1984. *Elastic instability phenomena*. Chichester, UK: Wiley.

Thompson, J. M. T., J. W. Hutchinson, and J. Sieber. 2017. "Probing shells against buckling: A non-destructive technique for laboratory testing." *Int. J. Bifurcation Chaos* 27 (14): 1730048. https://doi.org/10.1142/S0218127417300488.

Timoshenko, S. P., and J. Gere. 1961. *Theory of elastic stability*. New York: Dover Publications.

Tissot-Daguette, L., H. Schneegans, E. Thalmann, and S. Henein. 2022. "Analytical modeling and experimental validation of rotationally actuated pinned-pinned and fixed-pinned buckled beam bistable mechanisms." *Mech. Mach. Theory* 174 (Aug): 104874. https://doi.org/10.1016/j.mechmachtheory.2022.104874.

Virgin, L. N. 1986. "Parametric studies of the dynamic evolution through a fold." *J. Sound Vib.* 110 (1): 99–109. https://doi.org/10.1016/S0022-460X(86)80077-3.

Virgin, L. N. 2007. *Vibration of axially-loaded structures*. Cambridge, UK: Cambridge University Press.

Virgin, L. N. 2017. "On the flexural stiffness of 3D printer thermoplastic." *Int. J. Mech. Eng. Educ.* 45 (1): 59–75. https://doi.org/10.1177/0306419016674140.

Völlmecke, C., M. Todt, and S. Yiatros. 2021. "Buckling and postbuckling of architectured materials: A review of methods for lattice structures and metal foams." *Compos. Adv. Mater.* 30 (Jan): 26349833211003904. https://doi.org/10.1177/26349833211003904.

Wang, Q., H.-L. Zou, and Z.-C. Deng. 2020. "Snap-through of a pinned-clamped elastica with arbitrarily movable support at the clamped end." *Mech. Res. Commun.* 110 (Dec): 103617. https://doi.org/10.1016/j.mechrescom.2020.103617.

Xia, Y., M. Ruzzene, and A. Erturk. 2019. "Dramatic bandwidth enhancement in nonlinear metastructures via bistable attachments." *Appl. Phys. Lett.* 114 (9): 093501. https://doi.org/10.1063/1.5066329.

Yang, Y. B., L. J. Leu, and J. P. Yang. 2007. "Key considerations in tracing the postbuckling response of structures with multi winding loops." *Mech. Adv. Mater. Struct.* 14 (3): 175–189. https://doi.org/10.1080/15376490600723578.

Zhang, Y., Q. Wang, M. Tichem, and F. van Keulen. 2020. "Design and characterization of multi-stable mechanical metastructures with level and tilted stable configurations." *Extreme Mech. Lett.* 34 (Jan): 100593. https://doi.org/10.1016/j.eml.2019.100593.

Zhong, J., L. N. Virgin, and S. D. Ross. 2018. "A tube dynamics perspective governing stability transitions: An example based on snap-through buckling." *Int. J. Mech. Sci.* 149 (Dec): 413–428. https://doi.org/10.1016/j.ijmecsci.2017.10.040.